

II) once energy-matching corrections between metal d and chromophore levels is accounted for.

Conclusions

The very low photoionization He II cross section of the sulfur-based MOs when compared to the metal-based ones leads us to an efficient identification of the very complicated spectral pattern. In a similar manner, the PE bands associated with the chromophore levels interacting with the d metallic AOs (those of g symmetry) have been identified, so providing an estimate of the complexation perturbations by comparison with the bands of the noninteracting levels (u symmetry). The

set of Δn_- , Δn_+ , $\Delta \pi_+$, and $\Delta \pi_-$ values obtained in this manner are consistent with the expected chemical behavior of the central metal atom and represent a first rough estimate of the differing σ - and π -bonding capabilities of the Ni, Pd, and Pt atoms.

Acknowledgment. We thank the CNR (Rome) for generous financial support to this research and Prof. E. Tondello for helpful suggestions.

Registry No. Metc, 3735-92-0; Zn(dtc)₂, 14324-55-1; Ni(dtc)₂, 14267-17-5; Pd(dtc)₂, 15170-78-2; Pt(dtc)₂, 15730-38-8.

Contribution from the Institute of Inorganic Chemistry, The Norwegian Institute of Technology, University of Trondheim, 7034 Trondheim-NTH, Norway, and Department of Chemistry, University of Oslo, Oslo 3, Norway

Infrared Emission Spectra of Alkali Chloroaluminates and Related Melts

JAN HVISTENDAHL,^{1a} PETER KLAEBOE,^{1b} ERLING RYTTER,^{1a} and HARALD A. ØYE*^{1a}

Received February 10, 1983

Infrared emission spectra of chloroaluminates and related melts have been recorded with a new technique using thick samples as reference. The molten salt is compressed between a polished nickel piston and a diamond IIA window, and the nickel sample container is sealed with gold O-rings. This system allows infrared emission to be recorded between 50 and 1500 cm⁻¹ up to 600 °C and with at least 3 atm of vapor pressure of the sample. The method has been utilized for structural investigations of AlkAlCl₄ (Alk = Li, Na, K, Rb, Cs), KMCl₄ (M = Al, Ga, In), AlkAl₂Cl₇ (Alk = Li, Na, K, Cs), CsGa₂Cl, and NaAlCl₄-Al₂Cl₆ melts. Increasing perturbation of a tetrahedral AlCl₄⁻ ion in the series Cs < Rb < K < Na < Li has been inferred from the activation of the totally symmetric stretching vibration, intensity variations in overtones and combination bands, and the position of the anion-cation mode. A scheme for assignment of vibrational transitions called Build Up by Symmetry Correlated Ligands (BUSCL) has been described and applied to the Al-Cl-Al-bridged Al₂Cl₇⁻ ion. It turns out that probably only Li⁺ is able to stabilize a bent bridge and that a linear or limp bridge is preferred with the larger alkali ions.

Introduction

Chloroaluminate melts may be defined as mixtures between aluminum chloride and other metal chlorides. Characteristic of these systems is the formation of complex anions, a feature that is the origin of the well-known acid-base variations and other unique properties. The chloroaluminates are interesting not only from a theoretical point of view but also because they can be utilized in industrial and preparative chemistry where the melts can act as electrolyte, solvent, or catalyst.

The most thoroughly investigated chloroaluminates are the aluminum chloride-alkali chloride melt mixtures. Some of the main features of these molten salts are summarized in Table I. The dominant aluminum species in the basic melts ($X_{\text{AlCl}_3} < 0.5$) is AlCl₄⁻. The acidic mixtures have low melting temperatures and bond properties intermediate between covalent and ionic as demonstrated by the formation of chloroaluminate polymers and an immiscibility gap.^{2,3} Potentiometric,⁴⁻⁶ vapor pressure,^{7,8} and Raman spectroscopic⁹⁻¹¹

studies have shown that AlCl₄⁻, Al₂Cl₇⁻, Al_nCl_{3n+1}⁻ ($n \geq 3$), and Al₂Cl₆ are present for $X_{\text{AlCl}_3} > 0.5$. From the Raman studies,⁹⁻¹¹ it has been concluded that AlCl₄⁻ has a tetrahedral structure, while Al₂Cl₇⁻ and Al₂Cl₆ are composed of two AlCl₄⁻ tetrahedra sharing one and two corners, respectively. Neither the structure nor the stoichiometry of Al_nCl_{3n+1}⁻ ($n \geq 3$) has been determined, but usually only $n = 3$ (i.e., Al₃Cl₁₀⁻) is assumed.

The Raman spectra of aluminum chloride-alkali chloride molten mixtures are well established,⁹⁻¹¹ while little is known about the complementary infrared (IR) spectra necessary for a complete vibrational analysis of the melt structures. Thus, the aim of this work has been to obtain the relevant IR spectra in order to get a better structural characterization of these systems.

Interesting features to be studied are perturbation of the anions by the alkali metal counterions and whether the Al-Cl-Al bridges are linear or bent. The latter is the case in solids containing Al₂Cl₇⁻ or the corresponding bromide ion, Al₂-Br₇⁻.¹²⁻¹⁵ Furthermore, vibrations arising from ionic bonds can only be observed in the IR spectra.¹⁶ Such IR bands have

- (1) (a) University of Trondheim. (b) University of Oslo.
- (2) Fannin, A. A., Jr.; King, L. A.; Seegmiller, D. W.; Øye, H. A. *J. Chem. Eng. Data* **1982**, *27*, 114.
- (3) Carpio, R. A.; Fannin, A. A., Jr.; Kibler, F. C., Jr.; King, L. A.; Øye, H. A. *J. Chem. Eng. Data* **1983**, *28*, 34.
- (4) Torsi, G.; Mamantov, G. *Inorg. Chem.* **1972**, *11*, 1439.
- (5) Fannin, A. A., Jr.; King, L. A.; Seegmiller, D. W. *J. Electrochem. Soc.* **1972**, *119*, 801.
- (6) Boxall, L. G.; Jones, H. L.; Osteryoung, R. A. *J. Electrochem. Soc.* **1973**, *120*, 223.
- (7) Øye, H. A.; Gruen, D. M. *Inorg. Chem.* **1964**, *3*, 836. With data from: Dewing, E. W. *J. Am. Chem. Soc.* **1955**, *77*, 2639.
- (8) Viola, J. T.; King, L. A.; Fannin, A. A.; Seegmiller, D. W. *J. Chem. Eng. Data* **1978**, *23*, 122.
- (9) Cyvin, S. J.; Klaeboe, P.; Rytter, E.; Øye, H. A. *J. Chem. Phys.* **1970**, *52*, 2776.

- (10) Torsi, G.; Mamantov, G.; Begun, G. M. *Inorg. Nucl. Chem. Lett.* **1970**, *6*, 553.
- (11) Rytter, E.; Øye, H. A.; Cyvin, S. J.; Cyvin, B. N.; Klaeboe, P. *J. Inorg. Nucl. Chem.* **1973**, *35*, 1185.
- (12) Allegra, G.; Casagrande, G. T.; Immirzi, A.; Porri, L.; Vitulli, G. *J. Am. Chem. Soc.* **1970**, *92*, 289.
- (13) Couch, T. W.; Lokken, D. A.; Corbett, J. D. *Inorg. Chem.* **1972**, *11*, 357.
- (14) Rytter, E.; Rytter, B. E. D.; Øye, H. A.; Krogh-Moe, J. *Acta Crystallogr., Sect. B* **1973**, *B29*, 1541.
- (15) Rytter, E.; Rytter, B. E. D.; Øye, H. A.; Krogh-Moe, J. *Acta Crystallogr., Sect. B* **1975**, *B31*, 2177.

Table I. Main Features of AlkCl-AlCl₃ Melts (Alk = Alkali Metal)

X _{AlCl₃}	0	0.50	0.667	0.75	0.8-0.9	1.00	
Bond properties		Ionic				Immiscibility gap	Covalent
Increasing acidity ^a		→					
Increasing liquidus temp ^b		→					
Stoichiometric composition	AlkCl	AlkAlCl ₄	AlkAl ₂ Cl ₇	AlkAl ₃ Cl ₁₀		AlCl ₃	
Melt equilibria	Cl ⁻	$\text{AlCl}_3 \rightleftharpoons \text{AlCl}_2^- \rightleftharpoons \text{AlCl}_4^-$	$\text{AlCl}_3 \rightleftharpoons \text{Al}_2\text{Cl}_7^-$	$\text{AlCl}_3 \rightleftharpoons (\text{Al}_3\text{Cl}_{10})^-$	$\text{AlCl}_3 \rightleftharpoons \text{Al}_2\text{Cl}_6(l)$	$\rightleftharpoons \text{Al}_2\text{Cl}_6(l)$	

^a Strong variation in pAlCl₃ (and pCl⁻) at X_{AlCl₃} = 0.5. ^b Eutectic melt compositions depend on alkali counterion. LiAlCl₄(s) and NaAlCl₄(s) melt incongruently.

been found for most of the molten salts that have been investigated thoroughly by IR spectroscopy. These bands are broad and are located in the far-IR region. They usually are classified as cation-anion vibrations of a quasi-lattice structure in the melts.¹⁷

Many properties of the aluminum chloride-alkali chloride melts are maintained when the alkali metal is exchanged with a pseudoalkali or group 2 metal or when gallium or indium is substituted for aluminum. Thus, additional knowledge about melt structure may be obtained by studying M^{III}Cl₃-MCl_n melts (M^{III} = Al, Ga, In; M = alkali, pseudoalkali, or group 2 metal) as well as corresponding gaseous complexes and solid compounds.

Generally, IR spectroscopy of molten salts requires more complicated experimental techniques than room-temperature liquids, and great efforts have been made to develop IR methods suitable for melts. Most of the IR spectroscopic work on molten salts is summarized in reviews by Devlin et al.,¹⁸ Hester,¹⁶ Devlin,¹⁹ and Volkov.²⁰ Bates²¹ and Sheppard²² have recently reviewed the use of Fourier transform IR emission spectroscopy in general. The chloroaluminates are particularly difficult to investigate due to the relatively high vapor pressures and the reactivity toward moisture and oxygen. Thus, the melts preferably should be enclosed in a container sealed with an optical window for passage of IR radiation.

Experimental Section

Apparatus. In order to obtain satisfactory IR spectra of molten salts in general and of the chloroaluminates in particular, the following requirements have to be satisfied: (a) The optical window must be transparent at least in the frequency range 50–700 cm⁻¹ at temperatures up to 400 °C. (b) Window and sample container must not react with the melts. (c) The window must seal the container to at least 3 atm of inner pressure. (d) The spectra of the vapor phase above the melts must not interfere with the melt spectra. (e) Thin melt films must be studied in transmission or in emission due to the expected high absorption coefficients.

These requirements are most easily satisfied in an emission experiment since only one window will be needed. A complete cell assembly and furnace for high-temperature emission studies have been described elsewhere,²³ but the central part specific for molten salt work is illustrated in Figure 1. The sample (C) is enclosed in a nickel container (A) equipped with a diamond window (E) and a gold ring

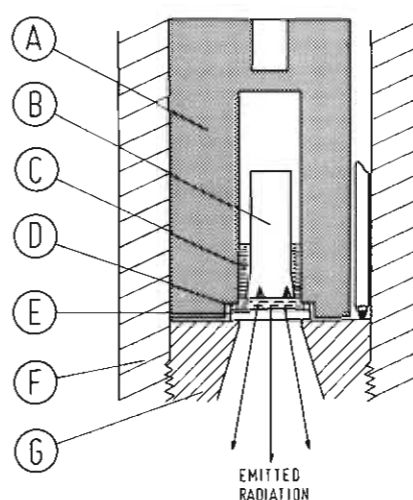


Figure 1. Cross section of the central part of the emission cell for molten salts: A, nickel sample container; B, nickel movable piston; C, melt; D, gold gasket; E, diamond window; F, stainless-steel outer cylinder; G, gold-plated stainless-steel support. The film thickness between the piston and the window is exaggerated for clarity.

seal (D). The container (A) and the support (G) is placed in an outer cylinder (F) of stainless steel that aligns the system and provides the pressure necessary to compress the gold ring from 0.5 to ca. 0.25 mm.

To obtain a sufficiently thin film of the molten salt (C), a movable piston (B) is pressed down into the melt by gravitational forces. The piston is made of nickel and has four grooves on the outer side where excess melt can flow. Nickel 213 (nearly pure nickel) is found suitable for aluminum chloride-alkali chloride mixtures.²⁴ The lower end of the piston acts simultaneously as a reflecting back-plate for the radiating sample, and it is ground with 1200-mesh emery paper and polished with 3- and 1- μm diamond powder on rotating disks. Between experiments, slight polishing by a cloth usually was sufficient.

The window (E) is of type IIa diamond (D. Drukker & Zn.) with 8-mm diameter and 1-mm thickness. Diamond IIa is nonabsorbing below approximately 1500 cm⁻¹ and 600 °C²³ and is less reactive than the other forms of carbon. Diamond does not react with chloroaluminum melts. The mechanical strength of diamond allows the sample container to be sealed to the window by a gold gasket. Other advantages of diamond as a window material are the very high thermal conductivity and the possibility of visual inspection of the melt during the experiment.

A Bruker IFS 114c IR Fourier transform spectrometer was available for the present study. This instrument can be evacuated to less than 0.1 torr, and lengthy purging after change of beamsplitter, detector, etc. therefore is avoided. As the beam is focused on the beamsplitters, these are small and easy to change compared to most other interferometers. The modular design of the spectrometer is convenient and permitted us to remove the sample compartment during the

- (16) Hester, R. E. *Adv. Molten Salt Chem.* **1971**, *1*, 1.
 (17) Wilmschurst, J. K. *J. Chem. Phys.* **1963**, *39*, 1779.
 (18) Devlin, J. P.; Li, P. C.; Cooney, R. P. J. In "Molten Salts"; Mamantov, G., Ed.; Marcel Dekker: New York, 1969; p 209.
 (19) Devlin, J. P. *Adv. Infrared Raman Spectrosc.* **1976**, *2*, 153.
 (20) Volkov, S. V. *Rev. Chim. Min.* **1978**, *15*, 59.
 (21) Bates, J. B. In "Fourier Transform Infrared Spectroscopy"; Ferraro, J. R., Basile, L. J., Eds.; Academic Press: New York, 1978; Vol. 1, p 99.
 (22) Sheppard, N. In "Analytical Applications of FT-IR to Molecular and Biological Systems"; Durig, J. R., Ed.; D. Reidel: Dordrecht, Holland, 1980; p 125.
 (23) Rytter, E.; Hvistendahl, J.; Tomita, T. *J. Mol. Struct.* **1982**, *79*, 323.

- (24) Brockner, W.; Tørklep, K.; Øye, H. A. *Ber. Bunsenges. Phys. Chem.* **1979**, *83*, 1.

emission work. As a consequence we avoided four mirrors employed in transmission spectroscopy and therefore reduced reflection losses. Also, a window may be mounted between the source compartment and the interferometer to protect the latter against corrosive vapors if a leak should occur in the cell. It was possible to mount the furnace permanently on the standard optical bench of the source compartment.²³ A flat mirror had to be included to direct the emitted radiation toward the focusing optics. Conventional detectors of TGS (triglycine sulfate) were employed.

Materials. All anhydrous salts were handled in an N₂-filled drybox (H₂O content <2 ppm) or under vacuum (pressure <10⁻⁵ torr). The binary salt mixtures LiAlCl₄, LiAl₂Cl₇, KInCl₄, and CsGa₂Cl₇ were obtained from previous spectroscopic work.^{11,25,26}

Two qualities of AlCl₃ were employed. For preparation of NaAlCl₄, NaAl₂Cl₇, and NaAl₃Cl₁₀, Al chips, purity 99.998% (Vigeland Brug), reacted at 450 °C with a flow of dry HCl from a HCl generator (NaCl + H₂SO₄). Aluminum chloride (Fluka) was used for the other samples. In both cases, the aluminum chloride was purified by repeated vacuum distillations.

The alkali chlorides NaCl (p.a., Merck), KCl (p.a., Baker), and RbCl (p.a., Merck) were recrystallized from the melts. The procedure for CsCl (p.a., Merck) included dehydration with HCl at 400 °C, chlorination of the molten salt, and double recrystallization.

The mixtures containing AlCl₃ were prepared as follows: Proper amounts of alkali chloride and aluminum chloride were weighed in a drybox and transferred to a silica tube furnished with a silica frit. The tube was sealed under vacuum, and the chlorides were mixed in the molten state. Aluminum chloride was distilled off to the tube's cooler end, which had been pulled out of the Kanthal-wound silica furnace. The remaining melt, which was approximately equimolar, was heated to about 500 °C and kept for several days to flocculate impurities. The temperature was then lowered, and the excess AlCl₃ was distilled back. After mixing, the melt was filtered. Melts that did not correspond to congruent melting compounds were quenched in liquid nitrogen to minimize phase separations. KGaCl₄ was prepared in a similar way except that the equimolar melt was not held at an elevated temperature for a prolonged time. The GaCl₃ (Merck) was used without further purification.

The tubes with the ready-made samples were opened in a drybox. Small portions (10–200 mg), each sufficient for one experiment, were placed in silica tubes and sealed vacuum tight.

Measuring Procedures. First, the outer cylinder (F) of the emission cell in Figure 1 was placed in the furnace, and the furnace and the flat mirror beneath were adjusted with a small light bulb at the top of the cylinder. Two pinholes were located at the sample position in the cylinder and at the focus between the source and interferometer compartments, respectively. Correct adjustment was examined visually by checking proper overlap of the two beams from the interferometer at all focal points and also overlap of the reflected beams from the interferometer on the pinhole between the source and interferometer compartments. Later adjustments were limited to alignment of the interferometer before the measurements and adjustment of the detector position after detector changes.

The movable piston, window, sample container, and a new gold gasket were cleaned in aqueous ammonia, distilled water, and ethanol. These parts were wrapped in Al foil and dried at 300 °C overnight under a pressure of less than 10⁻² torr. The emission cell was charged with a sample, and the entire arrangement shown in Figure 1 was assembled in a drybox before transference to a special evacuation unit. After having employed a rotary pump for at least 30 min, the sample container was sealed under vacuum.

The filled cell was heated in the furnace. The melting of the solid sample, with excess melt flowing up along the movable piston, was observed with a small mirror. Formation of a homogeneous melt film was examined before the spectrometer was evacuated. A uniform film is important as gas bubbles lead to melts too thick for obtaining high-quality spectra. The thickness of the melts could qualitatively be estimated from the shapes and intensities of the strong bands in the emittance spectra with a blackbody as reference. A remedy often successful for too thick or inhomogeneous melts is to lift the cell

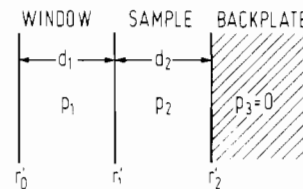


Figure 2. Sample between a back-plate and a window.

arrangement out of the furnace and turn it upside down a few times. The ideal sample thickness is probably below 10 μm.

The procedure for recording spectra of the thick samples employed as references was identical, except that no movable piston was used. The emission unit was charged with enough sample to make the melt at least 2 mm thick. A sooted cylindrical cavity, 24 mm deep and 6.2 mm wide, in a brass block was taken as the blackbody radiator. The outer dimensions of the block and its position in the emission unit were as for the sample container. Background spectra were measured with a piece of Al foil between the sample container and the screw supporting the window. The background was subtracted from the spectra of samples and references before emittances were calculated.

Principle

The emission setup for liquids with high vapor pressures consists schematically of a window, a sample, and a back-plate (Figure 2). The sample property of interest is the internal transmittance

$$p_2 = \exp(-K_2 d_2) \quad (1)$$

where K_2 is the absorption coefficient of the sample and d_2 is the thickness. It turns out, however, that the common emittance with a blackbody reference

$$\epsilon = I_{\text{sample}}/I_{\text{blackbody}} \quad (2)$$

with I equal to the measured intensities gives a poor representation of p_2 for strong bands.²⁵ Resulting band distortions are a consequence of the experimental difficulties involved because a small enough film thickness, d_2 , cannot be obtained.

The origin of the problem can be understood by considering a thick sample. Then the melt becomes opaque, and the emittance reaches the emissivity that is equal to

$$\epsilon' = I_{\text{opaque sample}}/I_{\text{blackbody}} = 1 - r_1' \quad (3)$$

(An ideal window has been assumed in the above equation, implying the reflectivity, r_0' , equal to zero and $p_1 = 1$.) The sample reflectivity, r_1' , for strong bands, varies considerably in the frequency range corresponding to a vibrational transition. In intermediate cases where the sample is not completely opaque, the bands with the highest absorption coefficients reach the $1 - r_1'$ limit. Thus, distortions and false splittings will occur in the spectra.

In a theoretical and experimental analysis of emission spectroscopy,²⁵ it has been shown that the annoying peak splittings are avoided by employing the new quantity

$$\epsilon^* = \epsilon/\epsilon' = I_{\text{sample}}/I_{\text{opaque sample}} \quad (4)$$

For an ideal window ($r_0' = 0$, $p_1 = 1$) and an ideal back-plate ($r_2' = 1$)

$$\epsilon^* \approx 1 - p_2^2 \quad (\text{strong bands, } p_2 \rightarrow 0) \quad (5)$$

and

$$\epsilon^* \approx (1 - p_2^2)/\epsilon' \quad (\text{weak bands, } p_2 \rightarrow 1) \quad (6)$$

As, however, ϵ' exhibits only small variations in the vicinity of weak bands, the emittance ϵ^* will in both cases give a good representation of the internal transmittance of the sample. Another important advantage of using ϵ^* is evident from (4). It is not necessary to establish an ideal blackbody since it will cancel out by using the relative quantity ϵ/ϵ' .

(25) Hvistendahl, J.; Rytter, E.; Øye, H. A. *Appl. Spectrosc.* **1983**, *37*, 182.

(26) Klæboe, P.; Rytter, E.; Sjøgren, C. E.; Tomita, T. *Proc. Soc. Photo-Opt. Instrum. Eng.* **1981**, *289*, 283.

(27) Tomita, T.; Sjøgren, C. E.; Klæboe, P.; Papatheodorou, G. N.; Rytter, E., to be submitted for publication.

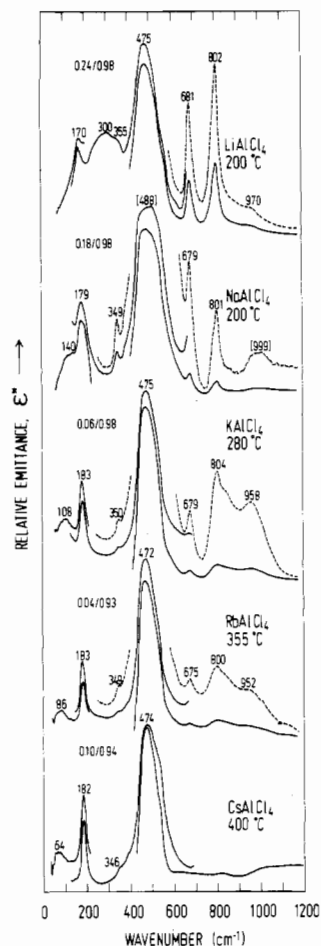


Figure 3. Infrared emission spectra of AlkAlCl_4 melts (Alk = Li, Na, K, Rb, Cs). The numbers divided by a slash are the lowest and highest emittances in the spectra recorded with a 3.5- μm beamsplitter (100–700 cm^{-1}). Opaque melts are references. Frequency of band center at 90% of peak height is given in brackets. --- refers to the expanded plot.

Results

Infrared emission spectra of the following melts have been recorded: AlkAlCl_4 (Alk = Li, Na, K, Rb, Cs) (Figure 3), KGaCl_4 and CsGa_2Cl_7 (Figure 4), $\text{AlkAl}_2\text{Cl}_7$ (Alk = Li, Na, K, Cs) (Figure 5), NaAlCl_4 - Al_2Cl_6 mixtures (Figure 6), and $\text{KInCl}_4(\text{l})$. Figure 4 includes the gas-phase spectrum of Ga_2Cl_6 recorded with a 0.5-mm gold spacer between the window and the back-plate.²⁶ With a few exceptions, the liquid spectra are presented in emittance, ϵ^* , with opaque melts as references. The well-developed peaks are marked with their frequencies, while the position of some strong peaks with irregular shapes around the maxima is given in brackets.

The beamsplitters employed and the approximate frequency ranges they cover were 12- μm Mylar (50–220 cm^{-1}), 3.5- μm Mylar (100–700 cm^{-1}), and Ge/KBr (400–4000 cm^{-1}). Some spectra were measured with a 23- μm Mylar (40–100 cm^{-1}) beamsplitter, but no additional information was found in these spectra. Because the beamsplitters have overlapping spectral ranges, the band positions, ν , were chosen as follows: $\nu < 150$ cm^{-1} with 12- μm Mylar, $150 < \nu < 200$ cm^{-1} as the mean position of 12- and 3.5- μm Mylar, $200 < \nu < 650$ cm^{-1} with 3.5- μm Mylar, and $650 < \nu$ with Ge/KBr. The minimum and maximum emittances of the spectra recorded with a 3.5- μm Mylar beamsplitter are given in Figures 3–6. Qualitatively, a high maximum emittance indicates a relatively thick melt. The frequencies for peaks and shoulders in the AlkMCl_4 and AlkM_2Cl_7 spectra are given in Tables II and III.

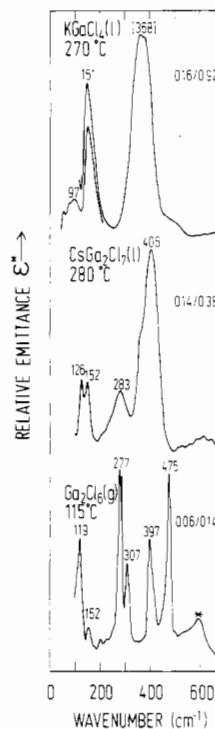


Figure 4. Infrared emission spectra of $\text{KGaCl}_4(\text{l})$, $\text{CsGa}_2\text{Cl}_7(\text{l})$, and $\text{Ga}_2\text{Cl}_6(\text{g})$. CsGa_2Cl_7 has blackbody reference. The reference for Ga_2Cl_6 is a blackbody at 200 °C and background radiation has not been subtracted. Asterisk denotes band due to background radiation. Further details are explained in the text to Figure 3.

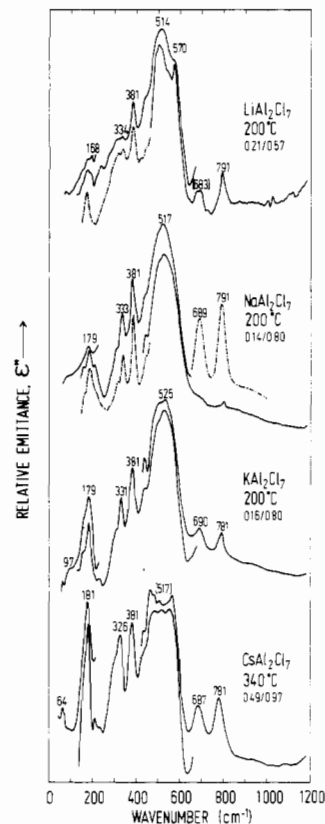


Figure 5. Infrared emission spectra of $\text{AlkAl}_2\text{Cl}_7$ melts (Alk = Li, Na, K, Cs): ---, spectra of different samples with a blackbody as reference in the frequency range 140–450 cm^{-1} . Further details are explained in the text to Figure 3.

All the spectra were recorded with a theoretical resolution of 8 cm^{-1} . Usually, 400 scans were collected and averaged before the Fourier transformation. Triangular apodization and

Table II. Infrared Frequencies of AlkMCl_4 Melts (Alk = Li, Na, K, Rb, Cs; M = Al, Ga, In)^a

LiAlCl_4 (200 °C)	NaAlCl_4 (200 °C)	KAlCl_4 (280 °C)	RbAlCl_4 (355 °C)	CsAlCl_4 (400 °C)	KGaCl_4 (270 °C)	KInCl_4 (340 °C)	assgnt ^d MCl_4^- (T_d)
300 s	140 m, sh	108 w	86 w	64 w	97 w		$\langle \text{Alk}^+ - \text{MCl}_4^- \rangle$
170 m	179 m	183 m	183 m	182 m	151 s	110 s	$\nu_4(\text{F}_2)$
355 vw, sh	349 w	350 vw	349 vw	346 vw, sh			$\nu_1(\text{A}_1)$
385 vw ^b	388 vw, sh		388 vw, sh	387 vw, sh			$\langle \text{Al}_2\text{Cl}_7^- \rangle$
475 vs	[488] vs ^c	475 vs	472 vs	475 vs	368 vs	323 vs	$\nu_3(\text{F}_2)$
					480 w, sh		$(\nu_2 + \nu_3)(\text{F}_1 + \text{F}_2)$
518 vw, sh		525 w, sh	520 w, sh	525 w, sh			$\langle \text{Al}_2\text{Cl}_7^- \rangle$
550 vw, sh							$(2\nu_1 - \nu_2)(\text{E})$
681 m	679 w	679 w	675 w				$2\nu_1(\text{A}_1)$
802 m	801 w	804 w	800 w	815 vw			$(2\nu_1 + \nu_2)(\text{E})$
970 vw, sh	[999] vw	958 vw	952 vw				$2\nu_3(\text{A}_1 + \text{E} + \text{F}_2)?$

^a vw = very weak, w = weak, m = medium, s = strong, vs = very strong, sh = shoulder; frequency of band center at 90% of peak height given in brackets. ^b Observed at higher temperatures. ^c The band position is probably shifted upward due to a too thick melt. ^d Frequencies not attributed to MCl_4^- given in angle brackets.

Table III. Infrared Frequencies of AlkM_2Cl_7 Melts (Alk = Li, Na, K, Cs; M = Al, Ga)^a

LiAl_2Cl_7 (200 °C)	NaAl_2Cl_7 (200 °C)	KAl_2Cl_7 (200 °C)	CsAl_2Cl_7 (340 °C)	CsGa_2Cl_7 (280 °C)	assgnt ^b M_2Cl_7^- (D_{3d})
		97 w, sh	64 w		$\langle \text{Alk}^+ - \text{Al}_2\text{Cl}_7^- \rangle$
		158 w, sh	165 w, sh	126 m	$\nu_{12}(\text{E}_u)$
168 m	179 m	179 m	181 m	152 m	$\nu_7(\text{A}_{2u})$
305 w, sh	310 w, sh	308 w, sh	304 w, sh		$\nu_2(\text{A}_{1g})$
334 w	333 m	331 m	326 m	283 m	$\nu_6(\text{A}_{2u})$
381 m	381 m	381 m	381 m	394 w, sh	$\nu_5(\text{A}_{2u})$
442 w, sh	440 w, sh	439 w	439 w, sh	366 w, sh	$\nu_1(\text{A}_{1g})$
514 vs	517 vs	525 vs	[517] vs	406 vs	$\nu_{11}(\text{E}_u)$
570 s (sh)					} M-Cl str
[683] w	689 w	690 w	687 w		
791 w	791 w	781 w	781 w		$(\nu_2 + \nu_5 + \nu_9)(\text{E}_u)$

^a See footnote to Table II. ^b The assignment of the M_2Cl_7^- bending modes is tentative. Angle brackets mark frequencies not attributed to M_2Cl_7^- .

sevenfold zero filling were employed. The single-beam spectra were stored on a magnetic disk for subsequent calculation of emittances.

Due to experimental difficulties, satisfactory determination of ϵ^* was not obtained for LiAl_2Cl_7 ($\nu < 250 \text{ cm}^{-1}$), NaAl_2Cl_7 ($\nu < 200 \text{ cm}^{-1}$), and CsGa_2Cl_7 over the entire frequency range. For these samples and frequency ranges, earlier spectra were utilized for which ϵ' had not been measured. Therefore, only ϵ could be calculated, but since the emittances are low, ϵ and ϵ^* are expected to give identical spectral information. The position of the 180-cm^{-1} band of $\text{NaAl}_3\text{Cl}_{10}$ was taken from the spectrum recorded with a $3.5\text{-}\mu\text{m}$ Mylar beamsplitter as the spectrum recorded with a $12\text{-}\mu\text{m}$ Mylar beamsplitter did not give reliable data for this band.

The uncertainty of the band positions is estimated to be $\pm 2 \text{ cm}^{-1}$ for narrow bands. For broad bands and well-defined shoulders, the uncertainty is $\pm 5 \text{ cm}^{-1}$, while it may be as high as $\pm 10 \text{ cm}^{-1}$ for the very strong and broad bands and less-defined shoulders. However, some of the broad bands probably are composed of several underlying peaks. The positions partly are dependent upon the melt thickness. This effect is seen for NaAlCl_4 (Figure 3) where the middle of the ν_3 band is at 488 cm^{-1} compared to the expected value of $\sim 475 \text{ cm}^{-1}$.

Discussion

AlkAlCl₄ Melts. From Raman spectroscopic⁹⁻¹¹ and potentiometric⁴⁻⁶ investigations it has been concluded that the dominant species in molten AlkAlCl_4 are Alk^+ and AlCl_4^- . The Raman spectra show four bands that correspond to the four fundamental modes of tetrahedral AlCl_4^- : $\nu_1(\text{A}_1) \approx 349 \text{ cm}^{-1}$, $\nu_2(\text{E}) \approx 120 \text{ cm}^{-1}$, $\nu_3(\text{F}_2) \approx 485 \text{ cm}^{-1}$, and $\nu_4(\text{F}_2) \approx 180 \text{ cm}^{-1}$. In $\text{LiAlCl}_4(\text{l})$, Rytter et al.¹¹ have reported a splitting of the $\nu_3(\text{F}_2)$ mode into three components at 473, 495, and 512 cm^{-1} . This splitting was ascribed to a lowering of the T_d symmetry of AlCl_4^- due to perturbation by the small and strongly polarizing Li^+ cation.

The spectroscopic consequences of perturbations from ideal tetrahedral symmetry have been studied in more detail for solid compounds containing the AlCl_4^- ion. In $\text{AlkAlCl}_4(\text{s})$, the anion is found to be only slightly distorted,²⁸ while large distortions appear for $\text{TiAl}_2\text{Cl}_8(\text{s})$ and $\text{TiAl}_2\text{Cl}_8 \cdot \text{C}_6\text{H}_6(\text{s})$.²⁹ The IR spectra of the titanium compounds revealed that the $\nu_3(\text{F}_2)$ mode of AlCl_4^- is split into two (466 and 552 cm^{-1}) and three (444, 505, and 554 cm^{-1}) components, respectively, and the IR-inactive $\nu_1(\text{A}_1)$ is activated. These observations are consistent with the crystal structures that show C_{3v} and C_{2v} distortions of AlCl_4^- .^{29,30}

The present infrared emission spectra of AlkAlCl_4 melts may be attributed to three structural features:

(1) **An Increased Perturbation of a Tetrahedral AlCl_4^- Ion in the Counterion Series $\text{Cs}^+ < \text{Rb}^+ < \text{K}^+ < \text{Na}^+ < \text{Li}^+$.** This conclusion can be inferred from the spectral details discussed below. (a) The $\nu_1(\text{A}_1)$ band around 350 cm^{-1} , which is IR inactive in T_d symmetry, is observed. Furthermore, the intensity increases with decreasing radius of the alkali ion. (b) Bands around 680, 800, and 550 cm^{-1} (the last for LiAlCl_4 only) appear with increasing intensities when the alkali ion becomes smaller. High intensities are specially marked in the lithium melt. These bands can be assigned to $2\nu_1$, $2\nu_1 + \nu_2$, and $2\nu_1 - \nu_2$, and they will only be IR active in a perturbed T_d configuration. (c) The $\nu_3(\text{F}_2)$ band around 475 cm^{-1} has a large bandwidth. This width may be taken as a sign of perturbational splitting of the triply degenerate T_d mode. Further, the band is observed from 5 to 20 wavenumbers lower in the IR than in the Raman spectrum. Such an apparent discrepancy may be due to different relative intensities of the ν_3 components in the IR and in the Raman spectrum. (d) The

(28) Mairesse, G.; Barbier, P.; Wignacourt, J.-P. *Acta Crystallogr., Sect. B* **1979**, *B35*, 1573.

(29) Justnes, H.; Rytter, E.; Andresen, A. F. *Polyhedron* **1982**, *1*, 393.

(30) Thewalt, U.; Stollmaier, F. *J. Organomet. Chem.* **1982**, *228*, 149.

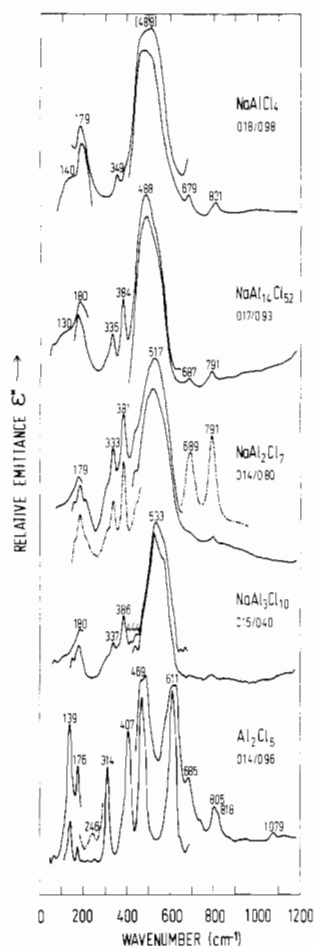


Figure 6. Infrared emission spectra of molten $\text{NaAlCl}_4\text{-Al}_2\text{Cl}_6$ mixtures at 200 °C: ---, spectra of different samples with a blackbody as references for NaAl_2Cl_7 in the frequency range 140–450 cm^{-1} . Further details are explained in the text to Figure 3.

$\nu_4(\text{F}_2)$ band is shifted to lower frequencies for LiAlCl_4 (170 cm^{-1} vs. $\approx 179 \text{ cm}^{-1}$). This is a bending mode, and the stronger polarizing power of a Li^+ counterion is expected to lower the Cl–Al–Cl bending force constant.

(2) **The Presence of Small Amounts of Al_2Cl_7^- Ions due to Dissociation of AlCl_4^- .** (c) The weak shoulders around 388 and 520 cm^{-1} may be attributed to Al_2Cl_7^- .

(3) **Quasi-lattice or Ion-Pair Alkali– AlCl_4 Interactions.** (f) The band that is shifted from 300 cm^{-1} for LiAlCl_4 to 64 cm^{-1} for CsAlCl_4 varies as expected for alkali–chlorine vibrations.

The following more detailed comments may be made with respect to the points a–f:

(a) All remarks regarding intensities are qualitative and are based on comparisons either within a given spectrum or between different spectra with appropriate bands as an internal standard.

The increased intensity of $\nu_1(\text{A}_1)$ with decreasing cation radius is most marked from $\text{KAlCl}_4(\text{l})$ to $\text{NaAlCl}_4(\text{l})$ (Figure 3). It may seem surprising that this fundamental is not more distinct for $\text{LiAlCl}_4(\text{l})$. However, the vibration appears as a shoulder on the very strong and broad LiAlCl_4 band centered at 300 cm^{-1} . The alternative assignment of the 350 cm^{-1} band as the IR-active overtone $2\nu_4$, which should be situated somewhat below 360 cm^{-1} , is unlikely since the intensity variation does not support this interpretation.

(b) It may be necessary to correct for anharmonicity when overtones are compared with fundamentals. The first overtone ($2\nu_1$) can be expressed in terms of the observed fundamental frequency by

$$2\nu_1 = [2(1 - 3x_e)/(1 - 2x_e)]\nu_1 \quad (7)$$

where x_e is the anharmonicity constant. By use of the typical Raman frequencies^{9–11} $\nu_1 = 349 \text{ cm}^{-1}$ and $\nu_2 = 120 \text{ cm}^{-1}$ and $x_e = 0.025$ for the anharmonicity constant of ν_1 , the calculated frequencies are $2\nu_1 = 680$, $2\nu_1 + \nu_2 = 800$, and $2\nu_1 - \nu_2 = 560 \text{ cm}^{-1}$. The comparison between calculated and observed frequencies (Table II) is very satisfactory and within the expected limits of error ($\pm 5 \text{ cm}^{-1}$). Although the fit depends upon a fairly large anharmonicity constant, the value employed (0.025) does not seem unreasonable. Further support for the assignments comes from the observation that the $2\nu_1 + \nu_2$ bands are stronger than those of $2\nu_1 - \nu_2$. In fact, the difference band is observed for LiAlCl_4 only. It is, however, remarkable that the intensities of the overtone are of the same magnitude as that of the fundamental.

Alternative explanations for the three bands above 600 cm^{-1} have to involve $\nu_3(\text{F}_2)$ or $\nu_4(\text{F}_2)$. The relevant combinations are IR active regardless of the symmetry of AlCl_4^- . Thus, no significant change in intensity with cation radius would be expected. Another argument against combinations involving ν_4 is the lack of the 9- cm^{-1} shift from $\text{LiAlCl}_4(\text{l})$ to $\text{NaAlCl}_4(\text{l})$. Neither is the broadness of the ν_3 band apparent in any of the three bands.

(c) An interpretation of the spectra in terms of splitting of $\nu_3(\text{F}_2)$ into separately observable components as in $\text{TiAl}_2\text{Cl}_8(\text{s})$ is rejected. This conclusion is *not* reached because we lack candidates in the spectra. In addition to the main peak at $\approx 475 \text{ cm}^{-1}$, we might consider the 385-, 518-, and 550- cm^{-1} bands (LiAlCl_4). It seems unreasonable, however, that the two extreme values originate from ν_3 since the splitting in the melts probably is smaller than for the solid titanium compounds (444–554 cm^{-1}).²⁹ The titanium aluminates have a more strongly polarizing counterion due to the higher charge and a 3d valence shell. The remaining frequencies at 475 and 518 cm^{-1} are close to the values 473 and 512 cm^{-1} reported for the Raman spectrum of LiAlCl_4 .¹¹ The expected reduced splitting with change to a larger alkali ion, however, is not found. Therefore, the 475- cm^{-1} frequency is assigned to $\nu_3(\text{F}_2)$ while the shoulder at 518 cm^{-1} is attributed to Al_2Cl_7^- .

(d) The shift of the $\nu_4(\text{F}_2)$ bending mode from 179 cm^{-1} for NaAlCl_4 to 170 cm^{-1} for LiAlCl_4 may be understood qualitatively from valence shell electron pair repulsion theory. The stronger polarizing Li^+ ion will pull the bonding electrons outward and create more ionic Al–Cl bonds. Hence, the force constant for Cl–Al–Cl bending is reduced.

(e) The shoulders attributed to Al_2Cl_7^- are near the detection limit, but nevertheless they are reproducible. It is somewhat surprising that they are observed as the anion fraction of Al_2Cl_7^- at exactly 50 mol % AlCl_3 is predicted to be 0.008 (LiAlCl_4 , 200 °C), 0.0004 (NaAlCl_4 , 200 °C), 0.0002 (KAlCl_4 , 280 °C), and 0.0002 (CsAlCl_4 , 400 °C). However, if the composition is changed to 50.2 mol % AlCl_3 , corresponding to the estimated uncertainty in composition of 0.2%, the Al_2Cl_7^- anion fraction increases to about 0.01.

(f) Detailed calculations for several anion–cation configurations by Wilson's FG matrix method³¹ reveals that the Li–Cl force constant is markedly stronger than for the heavier alkali ions. Thus, the shift of the alkali–chlorine frequency is not a pure mass effect. A higher force constant for Li is in good agreement with the most distinct perturbation of AlCl_4^- found for the LiAlCl_4 melt.

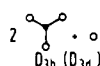
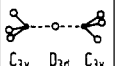
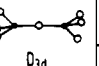
There are two previous IR studies of MAlCl_4 melts. Smyrl et al.³² presented the emission spectra of MAlCl_4 (M = Li, Na, K) and Gale and Osteryoung³³ studied the transmission

(31) Wilson, E. B., Jr.; Decius, J. C.; Cross, P. C. "Molecular Vibrations"; Dover Publications: New York, 1980.

(32) Smyrl, N. R.; Mamantov, G.; McCurry, L. E. *J. Inorg. Nucl. Chem.* **1978**, *40*, 1489.

(33) Gale, R. J.; Osteryoung, R. A. *Inorg. Chem.* **1980**, *19*, 2240.

Table IV. Vibrational Correlation Diagram for the Buildup of Al_2Cl_7^- from Two AlCl_3 Molecules and One Cl^- Ion^c

BASIS ^a	FREE COMPONENTS	SITE SYMMETRIES	FINAL ION	FINAL ASSIGNMENT WITH ORIGIN ^b		
$2\text{AlCl}_3 \cdot \text{Cl}^-$				$\text{Al}_2\text{Cl}_7^- (D_{3d})$		
	$D_{3h} (D_{3d})$	$C_{3v} D_{3d} C_{3v}$	D_{3d}	End group modes	Ligand librations	Skeletal modes
$2\nu_1 (393)$ $2R_z$ $2\nu_3 (619), 2\nu_4 (151), 2T_{xy}$	A_1^- A_2^- E_g^- A_1^-	A_2 A_2 E_g A_2	A_{1g} A_{2g} E_g A_{1u}	$\nu_1(\nu_1)(432), \nu_2(\nu_2)(151)$ $\nu_3(\nu_3)(-), \nu_4(\nu_4)(97)$	$[R_z]$ $\nu_{10}(R_{xy})(-)$ $\nu_6(R_z)(-)$	$\nu_7(T_2)(311)$ $[T_{xy}]$
$2\nu_2 (183), 2T_z$ $2R_{xy}$	A_2^- E_g^- E_g^-	A_2 E_g E_g	A_{2u} E_u E_u	$\nu_5(\nu_1)(381), \nu_7(\nu_2)(179)$ $\nu_1(\nu_3)(525), \nu_2(\nu_4)(158)$	$\nu_1(R_{xy})(-)$	$\nu_6(T_2)(331), [T_z]$ $\nu_{10}(T_{xy})(-), [T_{xy}]$
T_z T_{xy}	A_{2u} E_u	A_{2u} E_u				

^a Includes the vibrational, rotational, and translational degrees of freedom. Frequencies for matrix-isolated monomeric AlCl_3 are taken from ref 42 or 43. ^b The vibrational origin is given in square brackets and refers to the basis in column one. Observed frequencies in parentheses are for $\text{KAl}_2\text{Cl}_7(\text{l})$ (Table III and ref 11). Overall rotations and translations of Al_2Cl_7^- are eliminated. ^c -, IR activity allowed; --, Raman activity allowed.

spectrum of 1-butylpyridinium–aluminum chloride at room temperature. Due to reduced spectral quality and limited frequency ranges, none of these authors observed the lattice bands, the ν_1 peaks do not appear clearly, and ν_4 was not detected. On the other hand, there is good agreement between the emission studies regarding $2\nu_1$ and $2\nu_1 + \nu_2$. But, Smyrl et al.³² located the strongest band, ν_3 , for NaAlCl_4 and KAlCl_4 to 465 cm^{-1} compared to 475 cm^{-1} for KAlCl_4 in Table II. Since they used the back-plate as reference instead of a thick melt, the 10-cm^{-1} difference may well be due to the shift expected for ϵ when the melts are not ideally thin.²⁵

Molten KGaCl_4 and KInCl_4 . The IR spectra of KGaCl_4 (Figure 4) and KInCl_4 are as expected for tetrahedral GaCl_4^- and InCl_4^- ions. Of the four fundamental modes, only the IR-active $\nu_3(F_2)$ and $\nu_4(F_2)$ are observed. Compared to AlCl_4^- , any perturbational activation of $\nu_1(A_1)$ is difficult to detect because ν_1 is close to ν_3 . This overlap has been demonstrated in the Raman spectra of molten CsGaCl_4 ³⁴ and KInCl_4 ,³⁵ which gave ν_3 as a weak shoulder on ν_1 .

As expected, ν_3 becomes the strongest peak in the IR spectrum. The band positions are 368 and 323 cm^{-1} for GaCl_4^- and InCl_4^- vs. 375 and 347 cm^{-1} in the Raman spectra. The discrepancies, particularly for InCl_4^- , are not unexpected in view of the overlap of one strong and one very weak band in the Raman. The location of the bending mode ν_4 is within 3 cm^{-1} for the two techniques.

A band that is attributed to a cation–anion vibration was found at 97 cm^{-1} in the KGaCl_4 melt. The reduction from 108 cm^{-1} in KAlCl_4 might be a result of a weaker interaction in the gallium system, but a mass effect seems more likely. The frequency shift indicates that the group 3A metal also participates in the vibrations between the alkali ion and its surroundings.

The BUSCL Method. The basis for the vibrational classification of the Al_2Cl_7^- ion is chosen to be D_{3d} symmetry, i.e., a linear Al–Cl–Al bridge with a staggered arrangement of the end groups.¹¹ We are fully aware of the possibility that the symmetry of Al_2Cl_7^- may be lower, for instance by having a bent bridge similar to what is observed in solids.^{12,13} For simplicity, it is advantageous to employ a high symmetry as reference. The present treatment is useful not only if the symmetry is strictly D_{3d} but also if the bridge-bending force constant and the twisting constant are so low that the structure

is perturbed or fluctuates due to interionic interactions and thermal motions. Even the vibrations of an ion with a stable bent bridge may conveniently be described as a distorted D_{3d} ion.

The fundamentals are classified according to a Build Up by Symmetry Correlated Ligands (BUSCL) method.³⁶ The most straightforward scheme is obtained if the Al_2Cl_7^- ion is built up from two AlCl_3 molecules and one central Cl^- ion, but as an alternative we start with two AlCl_4^- ions and remove one Cl^- . Such a double approach has the advantage that it provides a check of the assignments.

The theoretical background for the symmetry treatment of equivalent ligands has been described elsewhere.³⁷ Previously reported applications to some organometallic compounds,³⁸ $(\text{C}_2\text{H}_5)_2$ ³⁹ and As_4O_6 ,⁴⁰ follow the procedure given below. Generally, the method consists of three stages: (A) As a starting point, the free ligands with their vibrational frequencies and corresponding symmetry representations are given. The translational and rotational motions also are included. (B) The ligands are given the proper site symmetries in the intermediate stage. (C) The final ion or molecule is built.

The vibrational analysis proceeds as follows:

(1) The transformations of the different representations are followed during the buildup. It is then possible to distribute the ligand modes between the different symmetry representations of the final ion or molecule.

(2) The vibrations are divided into end-group ligand modes, end-group librations, and skeletal modes.

(3) Motions associated with translation or rotation of the molecules as a whole are removed.

(4) If ions are removed, their corresponding degrees of freedom are eliminated.

(5) The observed frequencies are then correlated with the frequencies of the ligands, expecting numerical agreement between the final and original ligand frequencies. Intensity correlations are expected as well.

(6) Finally, the fundamentals of the built-up molecule or ion are numbered according to standard procedure.

(36) Rytter, E., to be submitted for publication.

(37) Rytter, E. *Chem. Phys.* **1976**, *12*, 355.

(38) Rytter, E. "Abstract of Papers", 170th National Meeting of the American Chemical Society, Chicago, IL, 1975; American Chemical Society: Washington, DC, 1975.

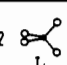
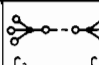
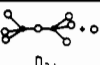
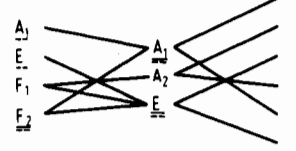
(39) Rytter, E.; Gruen, D. M. *Spectrochim. Acta, Part A* **1979**, *A35*, 199.

(40) Rytter, E.; Goates, S. K.; Papatheodorou, G. N. *J. Chem. Phys.* **1978**, *69*, 3717.

(34) Øye, H. A.; Bues, W. *Acta Chem. Scand., Ser. A* **1975**, *A29*, 489.

(35) Øye, H. A.; Rytter, E.; Klæboe, P. *J. Inorg. Nucl. Chem.* **1974**, *36*, 1925.

Table V. Vibrational Correlation Diagram for the Buildup of Al_2Cl_7^- from Two AlCl_4^- Ions with the Dissociation of One Cl^- ^c

BASIS ^a	FREE COMPONENTS	SITE SYMMETRIES	FINAL ION	FINAL ASSIGNMENT WITH ORIGIN ^b		
	2  T_d	 C_{3v} C_{3v}	 D_{3d}	$\text{Al}_2\text{Cl}_7^- (D_{3d}) + \text{Cl}^-$		
				End group modes	End group librations	Skeletal modes
$2\nu_1$ (350) $2\nu_2$ (122) $2R_{xyz}$ $2\nu_3$ (487), $2\nu_4$ (182), $2T_{xyz}$			A_{1g} A_{2g} E_g A_{1u} A_{2u} E_u	$\nu_1(\nu_3)(432), \nu_3(\nu_4)(161)$ $\nu_8(\nu_3)(-), \nu_9(\nu_2)(97)$ $\nu_5(\nu_1)(381), \nu_7(\nu_4)(179)$ $\nu_{11}(\nu_3)(525), \nu_{12}(\nu_2)(158)$	R_z $\nu_1, \nu_4(-)$ $\nu_6(R_z)(-)$ $\nu_3(\nu_4)(-)$	$\nu_2(\nu_1)(311), \text{Cl}^-$ R_{xy}, R_{yz} $\nu_6(\nu_3)(331), \text{Cl}^-$ $\nu_4(R_{xy})(-), \text{Cl}^-$

^a Includes the vibrational, rotational, and translational degrees of freedom. Frequencies for AlCl_4^- are taken from $\text{KAlCl}_4(l)$.¹¹ ^b See footnote *b* to Table IV. Vibrational modes of the hypothetical Cl-Cl bridge are crossed out when one Cl^- is dissociated. ^c See footnote *c* to Table IV.

Table IV shows the BUSCL method for the buildup of Al_2Cl_7^- from two AlCl_3 and one Cl^- . To the left, the translations, rotations, and vibrations of AlCl_3 and the corresponding symmetry representations are given. The translations of Cl^- are classified according to D_{3d} symmetry. The correlation during the buildup is followed by use of group correlation tables given for instance by Fateley et al.⁴¹ In the present case, the motions of AlCl_3 are divided into Raman-active gerade modes and partly IR-active ungerade modes. Because of this split, we expect that each gerade vibration in many instances will have an IR-active counterpart in the same frequency range.

The classification of frequencies into end-group modes, end-group librations, and skeletal modes is an approximation as none of them are purely of one category. Nevertheless, such a classification is helpful with respect to the later frequency assignments. The translations of the free components become skeletal modes, while the rotations are classified as ligand librations. The ligand vibrations transform simply into end-group modes. It is necessary to eliminate 6 degrees of freedom among the translations and rotations correlated from AlCl_3 . These 6 degrees of freedom correspond to translations and rotations of the ion as a whole. From the group-theoretical table for D_{3d} , it is seen that one mode from each of the representations $E_u, A_{2u}, E_g,$ and A_{2g} must be removed. The overall translations correspond to $T_{xy}(E_u)$ and $T_z(A_{2u})$ while the rotations are $T_{xy}(E_g)$ and $R_z(A_{2g})$. For instance, $T_{xy}(E_g)$ represents the degenerate linear combinations $T_{x1} - T_{x2}$ and $T_{y1} - T_{y2}$, where 1 and 2 specify the ligands, and $R_z(A_{2g})$ is $R_{z1} + R_{z2}$. It is evident that these coordinates give the proper rotations.

Table V gives the BUSCL method for the buildup of Al_2Cl_7^- from two AlCl_4^- and dissociation of one Cl^- . The buildup procedure parallels closely the previous case, but the classification in end-group modes, end-group librations, and skeletal modes is less obvious as one atom from each of the ligands jointly forms the central atom. This means that the central atom may be regarded as a dimer where one Cl^- is removed. As before, most of the skeletal vibrations have their origin in *T*, and *R* give the ligand librations, but exceptions occur for this special application of BUSCL.

Again, $T_{xy}(E_u), T_z(A_{2u}), T_{xy}(E_g),$ and $R_z(A_{2g})$ represent translation and rotation of the final ion. The modes that are removed due to the dissociation of one Cl^- are those associated with vibration and rotation of a Cl-Cl dimer. The corresponding Σ_g^+ and Π_g representations for a $D_{\infty h}$ dimer transform

to, respectively, A_{1g} and E_g in D_{3d} symmetry. Hence, the modes $T_z(A_{1g})$ and $R_{xy}(E_g)$ are removed.

It is seen that similar results are obtained for both buildups (Tables IV and V), and the expected six Raman-active and seven IR-active fundamentals are predicted for the $\text{Al}_2\text{Cl}_7^- (D_{3d})$ ion.

Assignment and Structures of Al_2Cl_7^- . Inspection of the spectra of molten AlAl_2Cl_7 (Figure 5) shows that the spectrum of KAl_2Cl_7 has the best signal to noise ratio, and this spectrum is used for the frequency assignments. The observed vibrational frequencies (in cm^{-1}) for molten KAl_2Cl_7 are as follows: IR 97 w, 158 w, 179 m, 308 w, 331 m, 381 m, 439 w, 525 vs, 690 w, 781 w; Raman 97 m, 161 m, 311 s, p, 432 w. All observed infrared frequencies are given, but the Raman frequencies are those observed by Rytter et al.¹¹ and assigned to the Al_2Cl_7^- ion.

As a basis for a structural interpretation, it is useful to obtain a probable vibrational classification of the observed bands. The frequencies that are not considered to originate from the fundamental modes of the Al_2Cl_7^- ion are sorted out first. Similar to the interpretation for molten MAICl_4 , an IR-active vibration due to $\text{K}^+-\text{Al}_2\text{Cl}_7^-$ interactions is expected. With reference to the $\text{M}^+-\text{AlCl}_4^-$ frequencies, the band at 97 cm^{-1} is ascribed to $\text{K}^+-\text{Al}_2\text{Cl}_7^-$. The corresponding $\text{Cs}^+-\text{Al}_2\text{Cl}_7^-$ band is found at 64 cm^{-1} .

It is unlikely that the peaks at 690 and 781 cm^{-1} belong to Al_2Cl_7^- fundamentals because the normal modes of KAlCl_4 and AlCl_3 with the highest frequencies are at 487 and 619 cm^{-1} , respectively.^{11,42} The former bands are considered as the combinations $(\nu_2 + \nu_5)(A_{2u})$ and $(\nu_2 + \nu_5 + \nu_9)(E_u)$ in D_{3d} symmetry. (See Table IV, column headed "end-group modes" regarding $\nu_2, \nu_5,$ and ν_9 .) These assignments give the following comparison between experimental and calculated frequencies: 690 vs. 692 cm^{-1} and 781 vs. 789 cm^{-1} . It is noteworthy that the combinations parallel closely the observations for AlCl_4^- . Table V gives the following correlations between the fundamentals for Al_2Cl_7^- and their AlCl_4^- origin: $\nu_2[\nu_1], \nu_3[\nu_1], \nu_9[\nu_2]$. Hence, the correspondence is $(\nu_2 + \nu_5)[2\nu_1]$ and $(\nu_2 + \nu_5 + \nu_9)[2\nu_1 + \nu_2]$, and indeed, $2\nu_1$ and $2\nu_1 + \nu_2$ are found for AlCl_4^- (Table II).

It remains to assign seven IR and four Raman bands. The BUSCL method is applied, and Tables IV and V are considered simultaneously when the observed Al_2Cl_7^- frequencies are related to the vibrations of the ligands. The guiding principle is that the value of the experimental frequencies should not be too far from the frequencies of their origin. In this way

(41) Fateley, W. G.; Dollish, F. R.; McDevitt, N. T.; Bentley, F. F. "Infrared and Raman Selection Rules for Molecular and Lattice Vibrations: The Correlation Method"; Wiley: New York, 1972.

(42) Pong, R. C. S.; Shirk, A. E.; Shirk, J. S. *Ber. Bunsenges. Phys. Chem.* **1978**, *82*, 79.

(43) Beattie, I. R.; Blyden, H. E.; Hall, S. M.; Jenny, S. N.; Ogdan, J. S. *J. Chem. Soc., Dalton Trans.* **1976**, 666.

it is possible to account satisfactorily for all frequencies except the two weak IR bands at 308 and 439 cm^{-1} . The results are given in the tables. In spite of the fact that none of the modes are strictly those of their origin, the assignments may be performed with a certain amount of confidence, especially since two schemes are used. It is, for instance, interesting that both procedures predict that $\nu_7(A_{2u})$ should be at a higher frequency than $\nu_{12}(E_u)$.

Some of the optically active modes have not been detected. The skeletal $\nu_{14}(E_u)$ bridge bending is not observed due to a weak intensity and a low frequency. The unobserved ligand librations are expected to be at low frequencies, but it cannot be completely excluded that ν_{13} should be assigned to either the 158- cm^{-1} or the 179- cm^{-1} band.¹³ In a previous Raman work,¹¹ it was not possible to observe $\nu_8(E_g)$. This mode has the ν_3 frequencies of AlCl_3 and AlCl_4^- as origin, and both have very low Raman intensities.^{11,42} Thus, the reason $\nu_8(E_g)$ remained unobserved is probably low intensity. Its IR counterpart, $\nu_{11}(E_u)$, indeed is observed and gives the strongest IR band as do ν_3 of the origins. Several similar intensity relations exist.

As stated above, the two weak bands at 308 and 439 cm^{-1} cannot easily be attributed to Al_2Cl_7^- with D_{3d} symmetry. It is significant that both bands have frequencies close to the two Raman-active A_{1g} stretching modes. Their probable assignments therefore are $\nu_2(A_{1g})$ and $\nu_1(A_{1g})$, with the IR activity resulting from a perturbation of the D_{3d} symmetry. This interpretation is in agreement with the Ga_2Cl_7^- spectrum (Figure 4) with one D_{3d} Raman mode, $\nu_1 = 366 \text{ cm}^{-1}$,³⁴ observed in the IR spectrum at the same frequency. The ν_2 fundamental for the Ga_2Cl_7^- ion, expected at 266 cm^{-1} ,³⁴ may constitute a part of the broad IR band at 283 cm^{-1} .

The assignments for KAl_2Cl_7 are summarized in Table III. The observed frequencies for LiAl_2Cl_7 , NaAl_2Cl_7 , CsAl_2Cl_7 , and CsGa_2Cl_7 are classified accordingly in the table. Our results may be compared with the recent analysis of Manteghetti and Potier.⁴⁴ They studied several solids containing Al_2X_7^- ($\text{X} = \text{Cl}^-, \text{Br}^-, \text{I}^-$). As a reference compound they used $\text{KAl}_2\text{Br}_7^-$ (s), partly due to the well-known C_s anion symmetry.¹⁴ A correlation of our assignments from D_{3d} to C_s gives a classification of the vibrational motions that is very close to the interpretation reported for the solids. In addition, the smaller number of stretching modes in the molten state supports the D_{3d} reference for the melt model.

After the vibrational frequencies of Al_2Cl_7^- have been assigned, it is useful to examine the spectra in more detail for a closer structural discussion. It also will be demonstrated that one advantage of the BUSCL method is to allow a straightforward comparison between the Al_2Cl_7^- frequencies and their AlCl_4^- counterparts. From Table III it is seen that the $\nu_7(A_{2u})$ band is shifted from 168 cm^{-1} for LiAl_2Cl_7 to 179 cm^{-1} for NaAl_2Cl_7 . This feature is parallel to the shift of the corresponding $\nu_4(\text{AlCl}_4^-)$ band, which shifts from 170 to 179 cm^{-1} . The same explanation may be inferred; i.e., the strongly polarizing Li^+ creates a more ionic Al-Cl bond in the chloroaluminate ion. The shift again demonstrates that Li^+ interacts strongest with the chloroaluminate ions.

The weak bands at 308 and 439 cm^{-1} were ascribed to IR-activated A_{1g} frequencies resulting from a perturbation of the D_{3d} symmetry. A compatible explanation was found for the $\nu_1(A_1)$ band in AlCl_4^- probably due to a cationic distortion. For Al_2Cl_7^- , the perturbation may arise either as an unsymmetrical interaction between Alk^+ and an Al_2Cl_7^- ion with approximate D_{3d} symmetry or because of a bent bridge structure. In the first case, Alk^+ may be attached to terminal chlorines at one end of the Al_2Cl_7^- ion. An energetically

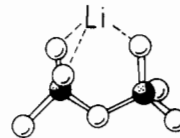


Figure 7. The $\text{Li}^+-\text{Al}_2\text{Cl}_7^-$ cage model.

favorable coordination of Alk^+ in the second case probably is to chlorine atoms from both the AlCl_3 end groups, thus giving a ring or cage structure (Figure 7). We tend to favor the first model for the heavier alkali ions and the last for Li^+ .

The $\nu_{11}(E_u)$ band shows a pronounced splitting into 514 and 570 cm^{-1} for LiAl_2Cl_7 . This observation is in contrast to the related LiAlCl_4 band, $\nu_3(F_2)$, or the other $\text{AlkAl}_2\text{Cl}_7$ melts where splitting is indicated only by large bandwidths. (The origin of the apparently irregular shape of the ν_{11} band for the cesium melt (Figure 5) is a too thick melt.) A probable interpretation seems to be that Li^+ may stabilize the bent bridge structure as shown in Figure 7 with an anion configuration as in solid $\text{Te}_4(\text{Al}_2\text{Cl}_7)_2$ and KAl_2Br_7 .^{13,14} Further support to this melt model comes from the four IR bands observed in $\text{Me}_4\text{NAl}_2\text{Cl}_7$ (s) between 526 and 560 cm^{-1} .⁴⁴ These frequencies for Al_2Cl_7^- with an assumed bent bridge have their origin in the doubly degenerate ν_8 and ν_{11} for a linear bridge (Tables IV and V). The splitting disappeared in organic, Friedel-Crafts solutions.⁴⁴ Thus, the reported changes for the solid-liquid transition correspond to the Li^+ -heavier Alk^+ substitution in the melts.

Gale and Osteryoung³³ point out that we have been reluctant to propose a bent Al-Cl-Al bridge because of the excessive number of vibrations predicted for such a structure over those found experimentally by Raman spectroscopy.¹¹ The present investigation makes it easier to concur with Gale and Osteryoung that a bent bridge is possible, at least for a strongly interacting counterion. Nevertheless, the present analysis demonstrates the advantage of using D_{3d} symmetry as a basis for frequency assignment, whether the actual symmetry is D_{3d} or lower. The present data make it probable that molten LiAl_2Cl_7 has a bent bridge through ring or cage formation. The other molten MAl_2Cl_7 compounds probably have a limp Cl bridge with random fluctuations around the linear configuration. A considerable angular flexibility of the bridge is supported by the corresponding ring-puckering mode of Al_2Cl_6 , which has a low force constant and a large vibrational amplitude.^{27,45}

Chloroaluminate Polymers. Higher anionic polymers, i.e., $\text{Al}_n\text{Cl}_{3n+1}^-$ ($n \geq 3$), are expected only in low concentrations.^{5,11} Furthermore, the polymer spectra will be obscured by the AlCl_4^- and Al_2Cl_7^- bands. It is therefore in accordance with the expectations that the spectra of the $\text{NaAlCl}_4-\text{AlCl}_3$ melts (Figure 6) show only a few features that may be attributed to $\text{Al}_n\text{Cl}_{3n+1}^-$.

One of these spectral characteristics is the gradual shift of the strongest peak from $\sim 475 \text{ cm}^{-1}$ for AlkAlCl_4 melts, through 517 cm^{-1} for NaAl_2Cl_7 (l), and to 533 cm^{-1} for $\text{NaAl}_3\text{Cl}_{10}$ (l). A similar, but reverse trend was found for the strong and polarized Raman band of the $\text{PCl}_5-\text{AlCl}_3$ system.⁴⁶ In addition, the $\text{NaAl}_3\text{Cl}_{10}$ melt gives rise to shoulders at 567 and 361 cm^{-1} , which may be due to the higher polymers. It is concluded that $\text{Al}_n\text{Cl}_{3n+1}^-$ ($n \geq 3$) species do exist in the aluminum chloride rich melt mixtures, but in low concentrations.

(45) Shen, Q. Ph.D. Thesis, Oregon State University, 1974.

(46) Poulsen, F. W. *J. Raman Spectrosc.* **1981**, *11*, 302.

(44) Manteghetti, A.; Potier, A. *Spectrochim. Acta, Part A* **1982**, *38A*, 141.

Acknowledgment. The authors are grateful to Claus J. Nielsen, Oslo, Norway, for his help with the FT-IR spectrometer and to Nansenfondet, NAVF, and NTNf for financial support.

Registry No. LiAlCl₄, 14024-11-4; NaAlCl₄, 7784-16-9; KAlCl₄, 13821-13-1; RbAlCl₄, 17992-02-8; CsAlCl₄, 17992-03-9; KGaCl₄, 18154-89-7; KInCl₄, 14323-44-5; LiAl₂Cl₇, 88453-49-0; NaAl₂Cl₇,

40368-44-3; KAl₂Cl₇, 67757-79-3; CsAl₂Cl₇, 88453-50-3; CsGa₂Cl₇, 12331-25-8; Al₂Cl₆, 13845-12-0.

Supplementary Material Available: A table of frequencies for the NaAlCl₄-Al₂Cl₆ spectra, including assignments of Al₂Cl₆ bands, and a figure showing IR emission spectra of KMCl₄ (M = Al, Ga, In) (2 pages). Ordering information is given on any current masthead page.

Contribution from the Department of Chemistry and Physics, Middle Tennessee State University, Murfreesboro, Tennessee 37132

Lewis-Base Properties of Ortho Chlorines in Copper(II) 2,4,6-Trichlorophenolates, 4-Bromo-2,6-dichlorophenolates, and 2,6-Dichlorophenolates As Studied by ³⁵Cl Nuclear Quadrupole Resonance Spectroscopy

GARY WULFSBERG,* JIM YANISCH, RON MEYER, JOHN BOWERS, and MARIA ESSIG

Received May 5, 1983

Several 2,4,6-trichlorophenolates of copper(II) for which X-ray crystallography has revealed weak ("secondary") bonding interactions of the metal and ortho chlorine have been studied by variable-temperature ³⁵Cl NQR. To aid in NQR frequency assignments, analogous 4-bromo-2,6-dichlorophenolates and 2,6-dichlorophenolates have also been synthesized and studied. The secondary-bonding chlorines have NQR frequencies from 0.8 to 2.2 MHz lower than those of the corresponding non-secondary-bonding ortho chlorines. Analysis of these figures using Townes-Dailey theory with some additional assumptions suggests the transfer or polarization of about 0.06 electron from Cl to (or toward) Cu. This figure is compared with corresponding data of T. L. Brown on electron transfer from the nitrogen donor atom of pyridine in its complexes. The NQR frequency lowerings are greater for the complexes *trans*-CuL₂(chlorophenolate)₂ (L = monodentate nitrogen ligand) than for *cis*-CuL'(chlorophenolate)₂ (L' = bidentate chelating nitrogen ligand). Anomalous temperature dependence of the NQR frequencies of the secondary-bonding chlorines is noted.

Introduction

Although the organic derivatives of most of the nonmetals (amines, phosphines, ethers and alcohols, sulfides and mercaptides, etc.) act as ligands in metal complexes, it is commonly presumed that the halocarbons are incapable of donating any of their unshared electron density to metal ions, even though the gas-phase basicity (proton affinity) of CH₃Cl is greater than that of, for example, CO.^{1,2} But there are cases in which a halocarbon has been found with its halogen atom apparently coordinated to a metal ion: the metal-halogen distance is within the sum of van der Waals radii of the metal and halogen atoms but is beyond the sum of the respective covalent radii. This type of weak interaction is commonly called secondary bonding.³⁻⁷ Its significance could be great in that the presence of weakly bonded ligands is often very desirable in catalysis by metal compounds.^{8,9}

Secondary bonding of a simple halocarbon to a metal compound has only been reported a few times.¹⁰⁻¹⁶ It is much

more likely if the halogen and the metal are present in the same organometallic molecule⁵⁻⁷ or if the halocarbon has another, stronger donor atom positioned so as to produce a chelating ligand.¹⁷ Of the crystallographically characterized examples of the latter class,¹⁸⁻²⁷ the largest number are 2,4,6-trichlorophenolates,²¹⁻²⁷ especially of copper(II).²³⁻²⁷ In each of the latter complexes one of the ortho chlorines of each

- Haney, M. A.; Franklin, J. L. *Trans. Faraday Soc.* **1969**, *65*, 1794.
- Haney, M. A.; Franklin, J. L. *J. Chem. Phys.* **1969**, *73*, 4328.
- Alcock, N. W. *Adv. Inorg. Chem. Radiochem.* **1972**, *15*, 1.
- Murray-Rust, P. *Mol. Struct. Diff. Methods* **1978**, *6*, 154.
- Prokof'ev, A. K.; Bregadze, V. I.; Okhlobystin, O. Yu. *Usp. Khim.* **1970**, *39*, 412; *Russ. Chem. Rev. (Engl. Transl.)* **1970**, *39*, 196.
- Furmanova, N. G.; Kuz'mina, L. G.; Struchkov, Yu. T. *J. Organomet. Chem. Libr.* **1979**, *7*, 153.
- Prokof'ev, A. K. *Usp. Khim.* **1976**, *45*, 1028; *Russ. Chem. Rev. (Engl. Transl.)* **1976**, *45*, 519.
- Stone, F. G. A. *Acc. Chem. Res.* **1981**, *14*, 318.
- Davies, J. A.; Hartley, F. R. *Chem. Rev.* **1981**, *81*, 79.
- Brown, H. C.; Eddy, L. P.; Wong, R. *J. Am. Chem. Soc.* **1953**, *75*, 6275.
- Brown, H. C.; Wallace, W. J. *J. Am. Chem. Soc.* **1953**, *75*, 6279.
- Thiebault, A.; Colin, J. P.; Oliva, P. *Anal. Lett.* **1977**, *10*, 429.
- Cook, P. M.; Dahl, L. F.; Dickerhoof, D. W. *J. Am. Chem. Soc.* **1972**, *94*, 5511.
- Cotton, F. A.; Ilesley, W. H.; Kaim, W. *J. Am. Chem. Soc.* **1980**, *102*, 3475.

- Baral, S.; Cotton, F. A.; Ilesley, W. H. *Inorg. Chem.* **1981**, *20*, 2696.
- Crabtree, R. H.; Faller, J. W.; Mellea, M. F.; Quirk, J. M. *Organometallics* **1982**, *1*, 1361.
- Smith, J. W. In "The Chemistry of the Carbon-Halogen Bond"; Patai, S., Ed.; Wiley: London, 1973; Part 1, p 265.
- Dwivedi, G. L.; Srivastava, R. C. *Acta Crystallogr., Sect. B: Struct. Crystallogr. Cryst. Chem.* **1971**, *B27*, 2316.
- Charbonnier, P. F.; Faure, R.; Loiseleur, H. *Acta Crystallogr., Sect. B: Struct. Crystallogr. Cryst. Chem.* **1978**, *B34*, 3598.
- Kuz'mina, L. G.; Bokii, N. G.; Struchkov, Yu. T.; Kravtsov, D. N.; Golovchenko, L. S. *Zh. Strukt. Khim.* **1973**, *14*, 508; *J. Struct. Chem. (Engl. Transl.)* **1973**, *14*, 463.
- Cingi, M. B.; Lanfredi, A. M. M.; Tiripicchio, A.; Reedijk, J.; Van Landschoot, R. *Inorg. Chim. Acta* **1980**, *39*, 181.
- Simonov, Yu. A.; Matuzenko, G. S.; Botoshanskii, M. M.; Yampol'skaya, M. A.; Gerbeleu, N. V.; Malinovskii, T. I. *Zh. Neorg. Khim.* **1982**, *27*, 407; *Russ. J. Inorg. Chem. (Engl. Transl.)* **1982**, *27*, 231.
- Vogt, L. H.; La Placa, S. J.; Bednowitz, A. L. American Chemical Society Meeting, Inorganic Division, San Francisco, March 1968, as reported in: Bullock, J. I.; Hobson, R. J.; Povey, D. C. *J. Chem. Soc., Dalton Trans.* **1974**, 2037.
- Wong, R. Y.; Palmer, K. J.; Tomimatsu, Y. *Acta Crystallogr., Sect. B: Struct. Crystallogr. Cryst. Chem.* **1976**, *B32*, 567.
- Ladd, M. F. C.; Perrins, D. H. G. *Acta Crystallogr., Sect. B: Struct. Crystallogr. Cryst. Chem.* **1980**, *B36*, 2260.
- Yampol'skaya, M. A.; Dvorkin, A. A.; Simonov, Yu. A.; Voronkova, V. K.; Mosina, L. V.; Yablokov, Yu. V.; Turte, K. I.; Ablov, A. V.; Malinovskii, T. I. *Zh. Neorg. Khim.* **1980**, *25*, 174; *Russ. J. Inorg. Chem. (Engl. Transl.)* **1980**, *25*, 94.
- Yablokov, Yu. V.; Simonov, Yu. A.; Yampol'skaya, M. A.; Dvorkin, A. A.; Matuzenko, G. S.; Voronkova, V. K.; Mosina, L. V. *Zh. Neorg. Khim.* **1980**, *25*, 2468; *Russ. J. Inorg. Chem. (Engl. Transl.)* **1980**, *25*, 1364.